

Received 3 April 2025, accepted 11 May 2025, date of publication 15 May 2025, date of current version 23 May 2025.

Digital Object Identifier 10.1109/ACCESS.2025.3570234



Modeling and Measurement of a Self-Oscillating Fluxgate Current Sensor for AC and DC Application

KUI XIONG^[0], CHANGXI YUE^[0], XIAODONG YIN¹, (Senior Member, IEEE), HAIBIN CHEN², AND HAOHAN ZHEN²

¹China Electric Power Research Institute, Wuhan 430074, China

Corresponding author: Kui Xiong (xiongkui@epri.sgcc.com.cn)

This work was supported by State Grid Corporation of China Science and Technology Project under Grant 5108-202218280A-2-409-XG.

ABSTRACT This paper studies fluxgate current sensors used for DC to high - frequency current measurement in various industrial fields. Traditional fluxgate technologies have drawbacks in circuit complexity and cost, while the self-oscillating fluxgate technology has model - related issues. An analytical model for the open-loop self-oscillating fluxgate circuit is developed. Key parameters affecting circuit performance are identified, and a trade-off between sensitivity and linear range is found. A three-core four-winding self-oscillating fluxgate sensor is proposed. Experimental results show that DC and power - frequency AC accuracy better than $\pm 0.1\%$, and high -frequency AC accuracy better than $\pm 1\%$ within 20kHz. This research provides useful insights for self-oscillating fluxgate current sensor design and optimization.

INDEX TERMS Self-oscillating fluxgate, current sensors, current measurement, output characteristic.

I. INTRODUCTION

Fluxgate current sensors, functioning as the AC/DC current transformers, are capable of measuring from currents ranging from DC to high - frequency. These sensors possess excellent performance in terms of accuracy, dynamic response, temperature stability, and long - term reliability. Consequently, they find extensive applications in various industrial fields such as renewable energy generation, electric vehicles, smart grids, and medical imaging for energy and current measurement [1], [2], [3], [4], [5], [6], [7], [8], [9].

The principle of fluxgate technology lies in the fact that when an excitation signal is applied to the core of the sensor, the resulting DC component induces even harmonics in the secondary windings. DC currents can be obtained by measuring the magnitude of these even harmonics through demodulation methods. Traditional fluxgate technology can be classified into phase-sensitive demodulation and peak-difference demodulation, depending on the different demodulation methods of the magnetic modulator. Since the 1950s,

The associate editor coordinating the review of this manuscript and approving it for publication was Yassine Maleh.

the theoretical basis and application research of fluxgate technology have been gradually established. F C. Williams and S W. Noble conducted research on the theoretical model of the phase-sensitive demodulation magnetic modulator. They employed graphical methods based on the segmented linearization models of magnetization curves to derive the output voltage equation of a dual-core magnetic modulator excited by triangular - wave signals. Moreover, they experimentally verified the sensitivity, noise, and error characteristics of this demodulation method [10]. E J. Kletsky utilized graphical methods to derive the output voltage equation of a magnetic modulator excited by trapezoidal-wave signals and analyzed the design principles of parameters such as excitation frequency, core size, and magnetic permeability [11]. Although these magnetic modulation techniques exhibit outstanding performance, the complexity of the demodulation circuits and high costs limit their widespread use.

In the early 1990s, M. Filanovsky proposed a novel method for measuring DC current. This method utilizes an RL multi-harmonic oscillation modulator composed of nonlinear transformers and operational amplifiers, which is known as the self - oscillating fluxgate technology. A linear relationship

²State Grid Shanghai Municipal Electric Power Company, Shanghai 200051, China



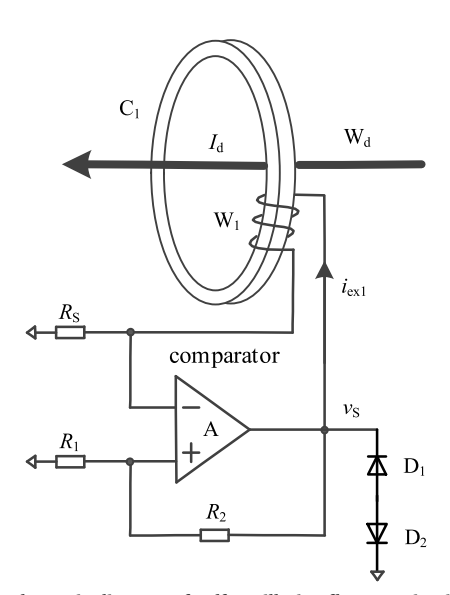


FIGURE 1. Schematic diagram of self-oscillating fluxgate circuit.

between the average excitation current and the input signal is established through the arctangent function model of the magnetization curve. However, due to the oversimplification of current parameters in the circuit, there is a significant deviation between the theoretical sensitivity and the experimental values [12], [13]. A three - winding self - oscillating fluxgate sensor was developed, which extended the measurement range to 700A and achieved a measurement accuracy of 0.2% [14]. Compared with traditional fluxgate technology, selfoscillating fluxgate technology still has a major drawback. The open - loop transfer function and sensitivity equation of the self - oscillating principle have not been effectively established. The existing segmented linear function models or arctangent function models based on magnetization curves are overly simplified, neglecting the influence relationships among important parameters such as the excitation signal and the number of windings turns. This makes it difficult to guide the design of fluxgate sensors to achieve optimal sensitivity and measurement accuracy.

In this paper, a four - winding self - oscillating fluxgate sensor is proposed, which can achieve high - accuracy measurement of both DC and high - frequency AC currents. The rest of the paper is organized as follows: In Section II, an analytical model for the open-loop self-oscillating fluxgate circuit is presented. The design and working principle of the proposed self-oscillating fluxgate sensor is discussed in Section III. Section IV conducts an experimental investigation of the output properties of the open - loop self - oscillating fluxgate circuit under different parameters, as well as the DC and AC errors of the proposed self - oscillating fluxgate sensor, and then analyzes the measurement results.

II. ANALYTICAL MODEL OF SELF-OSCILLATING FLUXGATE CIRCUIT

The self-oscillating fluxgate sensor is based on an RL-oscillating circuit for magnetic modulation of the

measured current signal. It incorporates a comparator circuit in positive - feedback mode and a nonlinear inductor, as shown in Figure 1. C₁ represents a core made of nonlinear ferromagnetic material with high magnetic permeability and low magnetic saturation strength. An excitation winding W₁ is evenly wound around it, forming a nonlinear inductor L with a winding resistance of $R_{\rm C}$. The voltage-dividing resistors R_1 and R_2 are used to set the forward threshold comparison voltage V⁺ and the reverse threshold comparison voltage V⁻. The output terminal of the RL self-oscillating circuit is connected in reverse-series with voltage stabilizing diodes D_1 and D_2 to set the peak excitation voltage U_S . The positive and negative peak values of the output voltage v_S of comparator A are symmetrical, i.e. $V_H = V^+ =$ $-V^-$. The sampling resistor R_S is employed to sample the excitation current signal iex. Wd is a primary winding, and its current magnitude is I_d . N_d and N_1 are the winding turns of the primary winding W_d and the excitation winding W₁, respectively.

When the self-oscillating fluxgate circuit is in operation, the magnetization curve of the excitation core C_1 and the variation of the excitation current $i_{\rm ex}$ are depicted in Figure 2. The simplified nonlinear excitation magnetization curve of core C_1 is represented by a three straight lines. The hysteresis effect can be ignored, because it cancels each other in two consecutive half cycles. The inductance of excitation winding W_1 is L and l respectively when the core C_1 operates in the linear and saturation regions. The positive saturation current of core C_1 is I_s , and the maximum excitation current of core C_1 is I_m . To make the excitation current generated by the self-excited oscillating circuit cause the core to enter the saturation region, there is $I_m > I_s$.

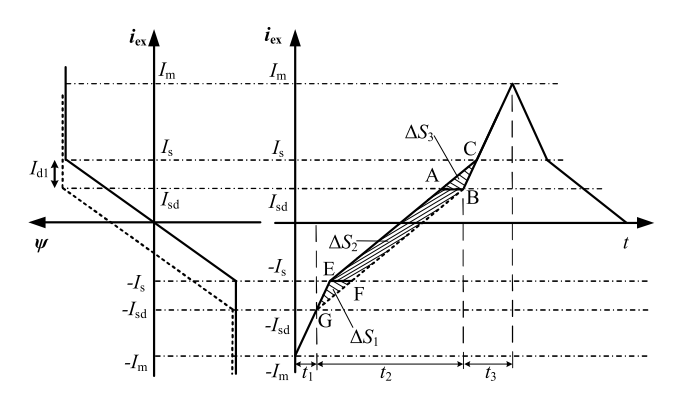


FIGURE 2. The magnetization curve and excitation current of the circuit.

When $I_{\rm d}=0$, the magnetization curve of the excitation core C_1 is completely symmetrical. The excitation current $i_{\rm ex}$ varies from the negative maximum excitation current $-I_{\rm m}$ to the positive maximum excitation current $I_{\rm m}$, passing through the GEAC point. At this point, the output voltage $v_{\rm S}$ of comparator A reversed, changing from $V_{\rm H}$ to $-V_{\rm H}$. Subsequently, the excitation current enters the next similar half cycle. According to the symmetry of the magnetization curve of nonlinear magnetic core C_1 , it can be inferred that the waveform of the excitation current $i_{\rm ex}$ is symmetrically



cancelled out by the positive and negative surrounding areas. Thus, the average value of i_{ex} in a complete cycle is zero.

When $I_{\rm d} > 0$, the magnetization curve of the excitation core C_1 is shown as the dashed line on the left of Figure 2. The excitation current required for the core C₁ to reach positive saturation is I_{sd} , where $I_{sd} = I_s - I_{d1}$ and $I_{d1} = (N_d/N_1)$ $I_{\rm d}$. Conversely, the excitation current required for negative saturation is $-I_{sd} = -I_s - I_{d1}$. The excitation current i_{ex} travels from the initial negative maximum excitation current $-I_{\rm m}$ to the positive maximum excitation current $I_{\rm m}$ passing through the GFBC point. The area enclosed by the positive and negative waveform of the i_{ex} changes by $-\Delta S$, where $-\Delta S = -(\Delta S_1 + \Delta S_2 + \Delta S_3)$ compared to the case when $I_{\rm d}=0$. The average value of the excitation current $i_{\rm ex}$ within a half-cycle is negative. The process of the next half-cycle is similar and will not be elaborated here. Therefore, by calculating ΔS and the half-cycle time $t=t_1+t_2+t_3$, the average output current value of the self-oscillating fluxgate circuit can be obtained.

According to Kirchhoff's voltage law, as shown in Fig.1, the circuit equations for the nonlinear iron core C_1 operating in the linear and saturation regions are:

$$v_{\text{ex}} = L \frac{di_{\text{ex}}(t)}{dt} + R_{\text{sum}} i_{\text{ex}}(t)$$

$$v_{\text{ex}} = L \frac{di_{\text{ex}}(t)}{dt} + R_{\text{sum}} i_{\text{ex}}(t)$$
(1)

where the total resistance on the excitation circuit is R_{sum} , i.e., $R_{\text{sum}} = R_{\text{S}} + R_{\text{W1}}$, and R_{W1} is the internal impedance of the excitation winding W_{1} .

As shown in figure 2, during the time $0 < t < t_1$, the nonlinear iron core C_1 operates in the negative saturation region of the magnetization curve. The inductance of the excitation winding W_1 is l, and the excitation voltage $v_{\rm ex} = V_{\rm H}$. Therefore, the differential equation for the excitation current $i_{\rm ex}$ during this period can be derived from equation (1) as follows:

$$V_{\rm H} = l \frac{di_{\rm ex}(t)}{dt} + R_{\rm sum} i_{\rm ex}(t) \tag{2}$$

The initial time of the above equation is t=0. With the initial condition $i_{\rm ex}$ (0) = $-I_{\rm m}$. Solving the current equation gives:

$$i_{\text{ex}}(t) = I_{\text{H}} - (I_{\text{H}} + I_{\text{m}})e^{-\frac{\tau}{\tau_1}}$$
 (3)

where $I_{\rm H}=V_{\rm H}/R_{\rm sum}$, $I_{\rm m}=\rho V_{\rm H}/R_{\rm s}$, $\rho=R_1/(R_1+R_2)$, and $\tau_1=l/R_{\rm sum}$.

Since the *t* is very small and approximately zero, the Taylor series of the equation (3) can be expanded to approximate the following equation:

$$i_{\rm ex}(t) = (I_{\rm H} + I_{\rm m}) \frac{tR_{\rm sum}}{I} - I_{\rm m}$$
 (4)

The slope of the GE line, i.e., the slope of the excitation current i_{ex} in the saturation region of the iron core, can be expressed as:

$$k_1 = (I_{\rm H} + I_{\rm m}) \frac{R_{\rm sum}}{l} = \frac{I_{\rm m} - I_{\rm s} - I_{\rm d1}}{t_1}$$
 (5)

The time t_1 can be solved as:

$$t_{1} = \frac{l}{R_{\text{sum}}} \left(\frac{I_{\text{m}} - I_{\text{s}} - I_{\text{d1}}}{I_{\text{H}} + I_{\text{m}}} \right) \tag{6}$$

During the time $t_1 \le t \le t_1 + t_2$, the core C_1 operates in the linear region of the magnetization curve. The inductance of the excitation winding W_1 is L, while the excitation voltage remains $v_{\rm ex} = V_{\rm H}$. The differential equation for the excitation current $i_{\rm ex}$ during this time can be obtained from the equation (1) as:

$$V_{\rm H} = L \frac{di_{\rm ex}(t)}{dt} + R_{\rm sum} i_{\rm ex}(t) \tag{7}$$

Solving the above equation with the initial condition, $i_{\rm ex}(t_1) = -I_{\rm s} - I_{\rm d1}$, gives the current equation:

$$i_{\rm ex}(t) = I_{\rm H} - (I_{\rm H} + I_{\rm s} + I_{\rm d1})e^{\frac{t_1 - t}{\tau_2}}$$
 (8)

Similarly, the Taylor series of the above equation can be approximated as:

$$i_{\rm ex}(t) = (I_{\rm H} + I_{\rm s} + I_{\rm d1}) \frac{tR_{\rm sum}}{L} - (I_{\rm H} + I_{\rm s} + I_{\rm d1}) \frac{t_1R_{\rm sum}}{L} - I_{\rm s} - I_{\rm d1}$$
(9)

The slope of the GB line, i.e., the slope of the excitation current i_{ex} in the linear region of the core, can be expressed as:

$$k_2 = (I_{\rm H} + I_{\rm s} + I_{\rm d1}) \frac{R_{\rm sum}}{I_{\rm s}} = \frac{2I_{\rm s}}{t_2}$$
 (10)

The time t_2 can be solved as:

$$t_2 = \frac{L}{R_{\text{sum}}} \left(\frac{2I_{\text{s}}}{I_{\text{H}} + I_{\text{s}} + I_{\text{d1}}} \right) \tag{11}$$

Similarly, based on the initial conditions of i_{ex} , the following equation can be obtained:

$$\frac{I_{\rm m} - I_{\rm s} + I_{\rm d1}}{t_3} = (I_{\rm H} - I_{\rm s} + I_{\rm d1}) \frac{R_{\rm sum}}{l} = k_3$$
 (12)

And the time t_3 can be solved as:

$$t_3 = \frac{l}{R_{\text{sum}}} \left(\frac{I_{\text{m}} - I_{\text{s}} + I_{\text{d1}}}{I_{\text{H}} - I_{\text{s}} + I_{\text{d1}}} \right)$$
(13)

In general circuit, there are $I_{\rm H} \gg I_{\rm m}$, $I_{\rm m} > I_{\rm s}$, $I_{\rm m} > I_{\rm d1}$. Combining equations (6), (11), and (13), t can be solved as:

$$t = t_1 + t_2 + t_3 = \frac{2I_s(L - l) + 2I_m l}{R_{\text{sum}} I_H}$$
 (14)

Also, $I_H \gg I_m$, $I_H \gg I_s$, $I_H \gg I_{d1}$. Combining equations (5), (10), and (12), k_1 , k_2 , k_3 can be solved as:

$$k_1 \approx k_3 = I_{\rm H} \frac{R_{\rm sum}}{l}$$

$$k_2 = I_{\rm H} \frac{R_{\rm sum}}{l} \tag{15}$$

Therefore, $\Delta S_1 \approx \Delta S_3$, and enlarged part of line ABC is shown in Figure 3, the line AB can be solved as:

$$AB = AD - BD = I_{d1} \frac{1}{k_2} - I_{d1} \frac{1}{k_3} = I_{d1} (\frac{L - l}{I_H R_{sum}})$$
 (16)

86432 VOLUME 13, 2025



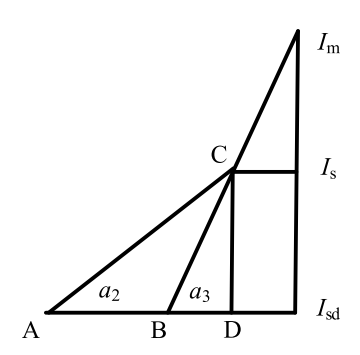


FIGURE 3. The enlarged part of line ABC.

The area of $\Delta S_1 + \Delta S_3$ is:

$$\Delta S_1 + \Delta S_3 = 2 \times \frac{1}{2} \times I_{d1} \times I_{d1} (\frac{L - l}{I_H R_{sum}}) = I_{d1}^2 (\frac{L - l}{I_H R_{sum}})$$
(17)

The area of ΔS_2 is:

$$\Delta S_2 = (2I_s - I_{d1}) \times I_{d1}(\frac{L - l}{I_H R_{sum}}) = 2I_s I_{d1}(\frac{L - l}{I_H R_{sum}})$$
$$-I_{d1}^2(\frac{L - l}{I_H R_{sum}})$$
(18)

Therefore, the area of ΔS is:

$$\Delta S = \Delta S_1 + \Delta S_2 + \Delta S_3 = 2I_s I_{d1} \left(\frac{L - l}{I_H R_{sum}}\right)$$
 (19)

Combining equations (14) and (19), the average output current can be derived as:

$$I_0 = \frac{\Delta S}{t} = \frac{I_{\rm s}I_{\rm d1}(L-l)}{I_{\rm s}(L-l) + I_{\rm m}l}$$
 (20)

Substituting $U_0 = I_0 R_{\text{sum}}$ and $I_{\text{d}1} = (N_p/N_1) I_d$, the sensitivity of the self-oscillating fluxgate circuit is:

$$S = \frac{dU_0}{dI_d} = \frac{R_{\text{sum}}}{N_1} \cdot \frac{I_{\text{s}}(L-l)}{I_{\text{s}}(L-l) + I_{\text{m}}l}$$
 (21)

If sensitivity S is differentiated with respect to the excitation current $I_{\rm m}$ to calculate the peak sensitivity:

$$\frac{dS}{dI_{\rm m}} = -\frac{R_{\rm sum}}{N_1} \cdot \frac{I_{\rm s}(L-l)l}{[I_{\rm s}(L-l) + I_{\rm m}l]^2} < 0 \tag{22}$$

The self-oscillating fluxgate circuit operates by leveraging the saturation nonlinear characteristics of the core, and $I_{\rm m} \geq I_{\rm s}$ must hold. Sensitivity decreases as $I_{\rm m}$ increases. Considering $L \gg l$, the theoretical maximum sensitivity $S_{\rm m}$ occurs when $I_{\rm m} = I_{\rm s}$, that is:

$$S_m = \frac{R_{\text{sum}}}{N_1} \tag{23}$$

According to equation (21), to increase circuit sensitivity, it is necessary to increase R_{sum} while decreasing I_{m} and N_1 . However, according to $I_sN_1 = H_sI$, when N_1 decreases, I_s will increase. To saturate the excitation core, I_{m} still needs to be increased. Overall, the impact of I_{m} on sensitivity should be smaller than that of R_{sum} and N_1 .

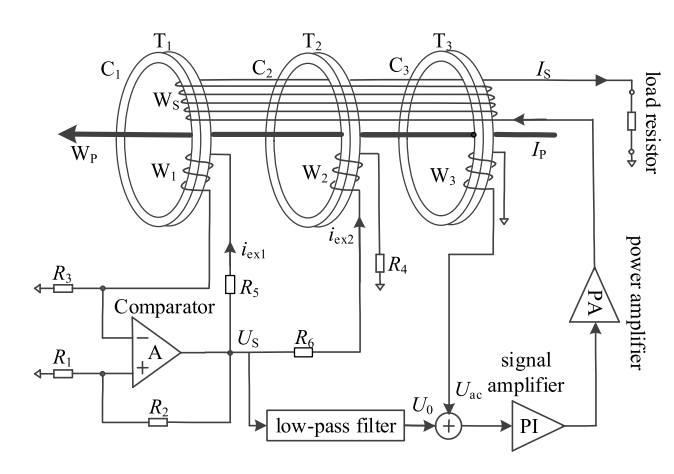


FIGURE 4. The Schematic diagram of the self-oscillating fluxgate sensor.

There exists a linear range equation for the self-oscillating fluxgate circuit [15]:

$$\frac{(-I_{\rm m} + I_{\rm s})N_1}{N_{\rm P}} \le I_{\rm d} \le \frac{(I_{\rm m} - I_{\rm s})N_1}{N_{\rm P}} \tag{24}$$

According to equation (24), to expand the linear range of the self-oscillating fluxgate circuit, excitation current $I_{\rm m}$ and the number of turns of the excitation winding $N_{\rm l}$ need to be increased. However, this contradicts the requirement for increasing sensitivity. Therefore, it is essential to comprehensively consider the reasonable parameter of the self-oscillating fluxgate circuit to achieve the optimal open-loop sensitivity and linear range.

III. PRINCIPLE OF THE SELF-OSCILLATING FLUXGATE SENSOR

Figure 4 shows the schematic diagram of a self-oscillating fluxgate sensor with a three-core and four-winding structure. The flux gate sensor consists of two DC magnetic coils, an AC magnetic coil, and a circuit module. The DC magnetic coil T_1 is composed of an excitation winding W_1 , a secondary winding W_S , and a core C_1 . The DC magnetic coil T_2 consists of an excitation winding W2, a secondary winding WS, and a core C₂. The AC magnetic coil T₃ is made up of an AC detection winding W₃, a core C₃, and a secondary winding W_S. The circuit module includes a self-oscillator, a low-pass filter, a signal amplifier, a power amplifier, and a load resistor. The self-oscillator is formed by threshold voltage setting resistors R_1 and R_2 , excitation current sampling resistors R_3 and R_4 , as well as comparator A. A nonlinear inductor L_1 is constituted by the core C₁ and the excitation winding W_1 , and a nonlinear inductor L_2 is formed by the core C_2 and the excitation winding W2. The self-oscillating circuit is composed of the self-oscillator and the nonlinear inductors L_1 and L_2 .

The principle of single core self-oscillating fluxgate circuit has been introduced in Section II and will not be repeated here. Due to the alternating magnetic flux generated by the excitation current I_{ex1} , high-frequency ripples will be induced



TABLE 1. Parameters of self-oscillating circuit.

PARAMETERS	Value
Core Material	nanocrystalline alloy
inner diameter/ outer diameter / thickness (mm)	48/51/3
$egin{array}{c} R_1 ackslash R_2 \ (\Omega) \end{array}$	220\ 5600



FIGURE 5. The self-oscillating fluxgate circuit test system.

in the secondary winding W_S . To compensate for the excitation magnetic flux, a reverse self-oscillating fluxgate circuit is set up. The excitation current I_{ex2} generates a reverse excitation magnetic flux in the iron core C_2 produced by the excitation voltage U_s . The cores C_1 and C_2 are made of the same magnetic material and are of the same size. The number of turns of the excitation winding W_1 and the excitation winding W_2 are the same, ensuring that the excitation magnetic fluxes in the cores C_1 and C_2 are equal in magnitude and opposite in phase. For the secondary winding W_S , the synthesized excitation magnetic flux caused by the cores C_1 and C_2 are zero simultaneously.

Due to the frequency-gain characteristics of the core and operational amplifier, the AC magnetic coil T3 can mainly amplify high-frequency signals and attenuate low-frequency signals. The output AC signal is added to the DC signal and then output to the power amplifier to drive the secondary winding WS. The secondary AC and DC current signals are generated in proportion to the primary winding WP, ultimately enabling the sensor to reach negative feedback zero-flux state. The secondary voltage signal is generated when the secondary current flows through the load resistor.

IV. EXPERIMENTAL TEST OF THE SELF-OSCILLATING FLUXGATE CIRCUIT

A. EXPERIMENTAL SETUP

The output characteristic equation (21) of the self-oscillating fluxgate sensor is obtained through theoretical analysis. When a specific ferromagnetic material is used for the core, the sensitivity of the fluxgate circuit is mainly related to three parameters: R_{sum} , N_1 , and I_{m} . To verify the effectiveness of

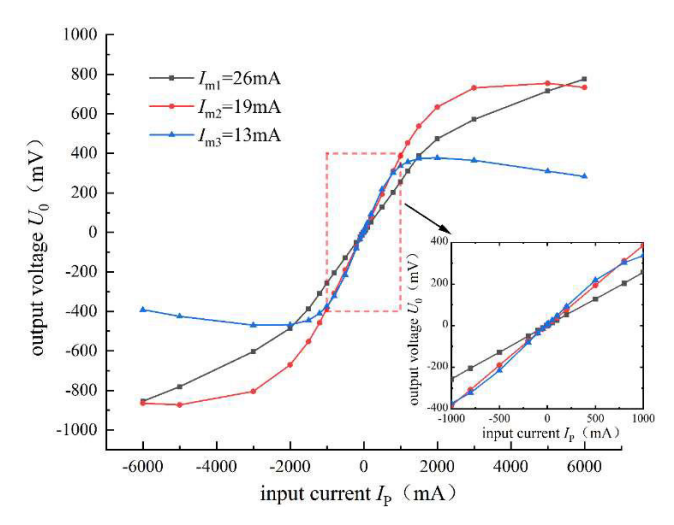


FIGURE 6. The output characteristic curve of different excitation current I_m .

the sensitivity equation of the self-oscillating fluxgate circuit, an open-loop test circuit was constructed, and each parameter is verified separately. The parameters of the self-oscillating fluxgate circuit are listed in Table 1.

The DC current source Fluke 5700 outputs a DC current of $10\text{mA}\sim6000\text{mA}$. The core is excited by a through winding current $I_{\rm p}$, and the output DC voltage U_0 is read out by an 8-digit digital multimeter Fluke 8508A. The excitation current $I_{\rm m}$ is sample by an oscilloscope with a resistor. The current $I_{\rm p}$ and the voltage U_0 correspond to the input and output signals required for the sampling. The image of the self-oscillating fluxgate circuit test system is shown in Fig. 5.

B. OUTPUT CHARACTERISTIC TESTING OF DIFFERENT EXCITATION CURRENT I_{M}

By adjusting the resistance value of R_1 to change the voltage ρV_H , and the excitation current I_m can be adjusted to $I_{\rm m1} = 26 \, \rm mA, \ I_{\rm m2} = 19 \, \rm mA, \ I_{\rm m3} = 13 \, \rm mA.$ The output characteristic curve of the self-oscillating fluxgate circuit, which represents the relationship between input current I_P and output voltage U_0 , is shown in Figure 6. It can be observed that the excitation current I_m has an impact on sensitivity. As shown in the enlarged figure, in the linear region, as the excitation current $I_{\rm m}$ decreases from large to small, the slope of the output characteristic line increases from small to large. When input current is in 200mA, the sensitivity of the circuit with $I_{\rm m1}=26{\rm mA}$ is 0.264V/A, the sensitivity of the circuit with $I_{\rm m2}=19{\rm mA}$ is 0.384V/A, and the sensitivity of the circuit with 0.467V/A. As excitation current $I_{\rm m}$ decreases, the sensitivity of the circuit increases, and this change in sensitivity is consistent with the theoretical equation. However, reducing $I_{\rm m}$ will also reduce the linear range. The linear range of the circuit with $I_{\rm m1}=26{\rm mA}$ is approximately ± 2000 mA, the linear range of the circuit with $I_{\rm m2}=19{\rm mA}$ is approximately \pm 1500mA, and the last one is approximately ± 1000 mA. The linear range of the output characteristic curve is approximately proportional to

86434 VOLUME 13, 2025



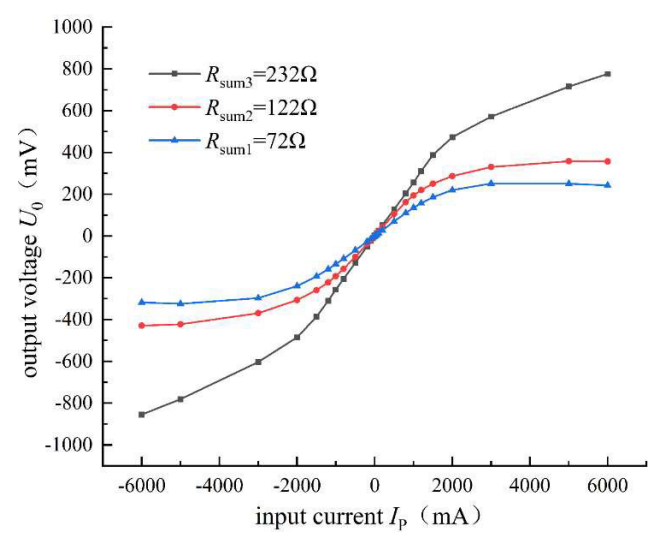


FIGURE 7. The output characteristic curve of different resistance R_{sum}.

 $I_{\rm m}$. Therefore, to obtain the desired linear range and high sensitivity, it is necessary to comprehensively consider the designated value of the excitation current $I_{\rm m}$.

C. OUTPUT CHARACTERISTIC TESTING OF DIFFERENT RESISTANCE R_{SUM}

When different values of R_{sum} , such as $R_{\text{sum}1} = 72\Omega$, $R_{\text{sum}2} = 122\Omega$, and $R_{\text{sum}3} = 232\Omega$, are selected, the relationship between the input current and the output voltage of the self-oscillating fluxgate circuit is measured, presented in Figure 6. The change of R_{sum} has a significant effect on sensitivity. Generally, the larger the value of R_{sum} , the higher the sensitivity will be. When the input current is within 1000mA, the input-output characteristic curve is in a linear region. The actual sensitivity can be calculated by the equation $S = U_0/I_p$. The values of S_1 , S_2 , and S_3 are 0.133V/A, 0.192V/A, and 0.256V/A respectively. However, according to the equation (23), the theoretical maximum sensitivities are 0.3V/A, 0.508V/A, and 0.967V/A respectively. When R_{sum} is small, the condition $I_{\rm H} \gg I_{\rm m}$ can be satisfied, and the values calculated by the theoretical equation are closer to the measured values, indicating a relatively high degree of approximation between S_m and S. Nevertheless, when the resistance R_{sum} increases, the current I_{H} will decrease, and the pre-condition $I_{\rm H} \gg I_{\rm m}$ cannot be met, ultimately resulting in a large deviation between the theoretical and the actual values of sensitivity.

D. OUTPUT CHARACTERISTIC TESTING OF DIFFERENT EXCITATION WINDING TURNS N₁

When different values of excitation winding turns N_1 , i.e. $N_{11} = 300$, $N_{12} = 400$, and $N_{13} = 500$ are chosen, the output characteristic curve of the self-oscillating fluxgate circuit is measured, as shown in Figure 8. The influence of the change of N_1 on sensitivity is such that the smaller the N_1 is, the higher the sensitivity will be. When the input current is within 500mA, the output characteristic curve is in the

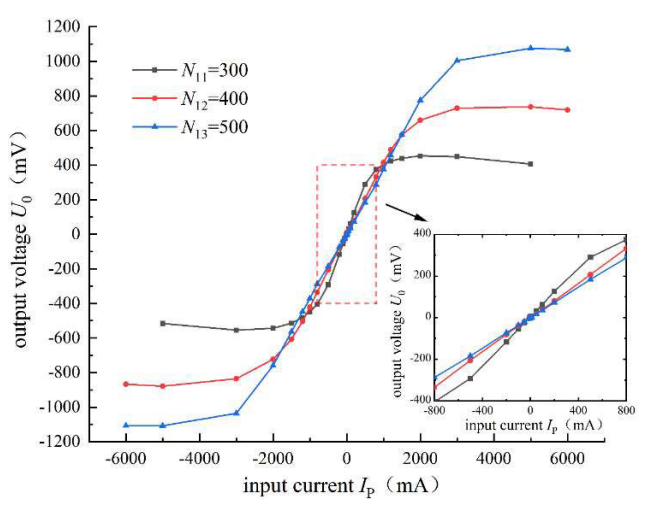


FIGURE 8. The output characteristic curve of different excitation winding

TABLE 2. Parameters of self-oscillating fluxgate sensor.

PARAMETERS	Value
Load resistor	4Ω
Rate primary current	500A
Rate second current	0.25A

linear region. Similarly, the actual sensitivities S_1 , S_2 , and S_3 can be calculated to be 0.584V/A, 0.411V/A, and 0.369V/A respectively. This shows that the actual sensitivity is inversely proportional to the number of turns N_1 , which is consistent with the theoretical equation (21). At the same time, the number of turns of the exciting winding N_1 directly affects the linear range. When the excitation winding turns are $N_{11} = 300$, $N_{12} = 400$, and $N_{13} = 500$, the linear range is 1000mA, ± 1500 mA, ± 2000 mA respectively. The linear range of the output characteristic curve is essentially proportional to N_1 . Therefore, when designing the number of turns of the exciting winding N_1 , it is necessary to simultaneously consider its impact on both the sensitivity and the linear range.

V. EXPERIMENTAL TEST OF THE SELF-OSCILLATING FLUXGATE SENSOR

A. EXPERIMENTAL SETUP

In this section, a prototype of self-oscillating fluxgate current sensor was built in accordance with the principles proposed above, as shown in Fig. 4. The experiments include DC errors, power-frequency AC errors, high-frequency AC errors, and frequency response measurements. The image of the constructed self-oscillating fluxgate sensor is presented in fig.9. The parameters of the self-oscillating fluxgate sensor are listed in Table 2.

B. DC ERROR MEASUREMENT

The current was provided by a Sorensen SGX power supply. Reference current readings were taken by a LEM IT 200-S





FIGURE 9. The image of the self-oscillating fluxgate sensor.

TABLE 3. Measurement DC error of the sensor.

Errors	Applied current % of rated current			
	5%	20%	100%	120%
f(%)	-0.061	0.054	-0.021	-0.028

TABLE 4. Measurement AC (50Hz) Error of the sensor.

Errors -	Арг	olied current	% of rated cur	rent
	5%	20%	100%	120%
f(%)	0.091	0.081	0.026	0.017
δ ($'$)	-0.03	0.36	0.21	0.14

transducer. Voltages were measured by Agilent 34465A digital multimeter. The resulting TABLE 3 shows the sensor's DC accuracy is better than $\pm 0.1\%$.

C. POWER-FREQUENCY AC ERROR MEASUREMENT

The 50Hz current was provided by an AC power supply. Reference current readings were taken using a standard current transformer. The accuracy of the standard current transformer at the power frequency is less than 0.01% and 0.3' from 5% to 120% of rated current. An AC current is applied to the primary windings of both the standard current transformer and the tested sensor, and then the test set measured the ratio error and the phase displacement by comparing the secondary currents of the two current transducers. The resulting TABLE 4 shows the sensor's power-frequency AC accuracy is better than $\pm 0.1\%$

D. HIGH-FREQUENCY AC ERROR MEASUREMENT

The High frequency current was provided by an Agilent 33220A signal generator and an AETECHRON 7796 power amplifier. Reference current readings were taken by a Fluke A40B precision AC Current shunt. The accuracy of the precision AC Current shunt within 100kHz is less than 0.01% and 0.3'. A 50A high-frequency AC current is applied to the primary windings of both the precision AC Current shunt and the tested sensor, and then the test set measures the ratio error and the phase displacement. The resulting TABLE 5 shows the sensor's high frequency AC accuracy within 20kHz is better than $\pm 1\%$.

TABLE 5. Measurement high frequency AC Error of the sensor.

Errors -		frequen	cy of applied	current	
	0.1kHz	1kHz	5kHz	10kHz	20kHz
f(%)	-0.035	-0.057	-0.283	-0.492	-0.785
δ(')	-0.4	-1.7	0.1	6.6	35.4

VI. CONCLUSION

This paper focuses on fluxgate current sensors, which are capable of measuring currents from DC to high- frequency ranges and are extensively applied in various industrial fields. Traditional fluxgate technologies, including phase - sensitive demodulation and peak - difference demodulation, have limitations in circuit complexity and cost.

The self-oscillating fluxgate technology, proposed in the 1990s, also has shortcomings such as inaccurate sensitivity models. To address these problems, an analytical model for the open-loop self-oscillating fluxgate circuit is developed. By analyzing the magnetization curve of the excitation core and employing the graphical method, equations for the excitation current in different regions are deduced, and expressions for circuit sensitivity are derived. It is found that parameters such as R_{sum} , N_1 , and I_{m} significantly influence the circuit performance, and there is a trade-off between sensitivity and linear range. The principle of the zero-flux CT in the proposed sensor is introduced. It adopts a three -core and four-winding structure, with reverse self-oscillating circuits utilized to compensate for excitation magnetic flux and an AC magnetic coil to amplify high-frequency signals, thereby achieving a negative - feedback zero - flux state. Experimental tests are carried out. Regarding the self-oscillating circuit, the impacts of different values of $I_{\rm m}$, $R_{\rm sum}$, and N_1 on sensitivity are verified. The experimental results are consistent with theoretical equations in trend, yet there are some deviations in actual values. For the self-oscillating fluxgate sensor, DC error, power - frequency AC error, and high - frequency AC error measurements are conducted. The sensor shows high accuracy, with DC and power-frequency AC accuracy better than $\pm 0.1\%$, and high-frequency AC accuracy better than $\pm 1\%$ within 20kHz. This research provides a valuable reference for the design and optimization of fluxgate current sensors.

REFERENCES

- S. Wei, X. Liao, H. Zhang, J. Pang, and Y. Zhou, "Recent progress of fluxgate magnetic sensors: Basic research and application," *Sensors*, vol. 21, no. 4, p. 1500, Feb. 2021, doi: 10.3390/s21041500.
- [2] T. Goktas, K. W. Lee, M. Zafarani, and B. Akin, "Analysis of magnet defect faults in permanent magnet synchronous motors through fluxgate sensors," in *Proc. IEEE Appl. Power Electron. Conf. Expo. (APEC)*, Long Beach, CA, USA, Mar. 2016, pp. 2875–2880, doi: 10.1109/APEC.2016.7468272.
- [3] N. Shtabel, L. Samotik, and E. Mizrakh, "Fluxgate direct current sensor for real-time insulation resistance monitoring," in *Proc. Int. Conf. Ind. Eng., Appl. Manuf. (ICIEAM)*, Sochi, Russia, Mar. 2019, pp. 1–5, doi: 10.1109/ICIEAM.2019.8743050.
- [4] F. Primdahl, "The fluxgate magnetometer," J. Phys. E, Sci. Instrum., vol. 12, no. 4, pp. 241–253, Apr. 1979, doi: 10.1088/0022-3735/12/4/001.

86436 VOLUME 13, 2025



- [5] D. M. Miles, M. Ciurzynski, D. Barona, B. B. Narod, J. R. Bennest, A. Kale, M. Lessard, D. K. Milling, J. Larson, and I. R. Mann, "Lownoise permalloy ring cores for fluxgate magnetometers," *Geosci. Instrum.*, *Methods Data Syst.*, vol. 8, no. 2, pp. 227–240, Sep. 2019, doi: 10.5194/gi-8-227-2019.
- [6] R. Pavel, B. Mattia, J. Fan, and X. Li, "Sensitivity and noise of wire-core transverse fluxgate," *IEEE Trans. Magnetics*, vol. 46, no. 2, pp. 654–657, Feb. 2010, doi: 10.1109/TMAG.2009.2033554.
- [7] A. V. Churyumov, A. N. Ermakov, and V. I. Torgashev, "Fluxgate current sensors for power electronics applications," in *Proc. IEEE Int. Conf. Elect. Mach. Syst.*, Beijing, China, Aug. 2011, pp. 1–4, doi: 10.1109/ICEMS.2011.6034595.
- [8] J. L. Sanchez-Ramos, J. M. Lopez-Garcia, and A. Fernandez-Cabanas, "Fluxgate current sensors for high-frequency applications in power electronics," in *Proc. IEEE Int. Symp. Ind. Electron.*, Vigo, Spain, Jun. 2007, pp. 134–139, doi: 10.1109/ISIE.2007.4285541.
- [9] P. K. Jain and A. K. Prasad, "Design and development of a fluxgate current sensor for power electronics applications," in *Proc. IEEE Int. Conf. Power Electron. Drive Syst.*, Singapore, Sep. 2005, pp. 1023–1028, doi: 10.1109/PEDS.2005.1554407.
- [10] F. Williams and S. Noble, "The fundamental limitations of the second-harmonic type of magnetic modulator as applied to the amplification of small DC signals," *Proc. IEE II, Power Eng.*, vol. 97, no. 58, pp. 445–459, Aug. 1950, doi: 10.1049/JIEE-2.1950.0112.
- [11] E. Kletsky, "Design criteria for low-level second-harmonic magnetic modulators," *Trans. Amer. Inst. Electr. Eng., I, Commun. Electron.*, vol. 77, no. 6, pp. 1013–1019, 1959, doi: 10.1109/tce.1959.6372933.
- [12] I. Filanovsky and V. Piskarev, "Sensing and measurement of DC current using a transformer and RL-multivibrator," *IEEE Trans. Circuits Syst.*, vol. 38, no. 11, pp. 1366–1370, Aug. 1991, doi: 10.1109/31.99166.
- [13] I. M. Filanovsky and L. Taylor, "Circuit with nonlinear transformer allowing DC current measurements via an isolation gap," in *Proc. 5th Midwest Symp. Circuits Syst.*, Aug. 1992, pp. 318–323, doi: 10.1109/MWS-CAS.1992.271296.
- [14] G. Velasco-Quesada, M. Roman-Lumbreras, and A. Conesa-Roca, "Design of a low-consumption fluxgate transducer for high-current measurement applications," *IEEE Sensors J.*, vol. 11, no. 2, pp. 280–287, Sep. 2011, doi: 10.1109/JSEN.2010.2054831.
- [15] P. Pejovic, "A simple circuit for direct current measurement using a transformer," *IEEE Trans. Circuits Syst. I, Fundam. Theory Appl.*, vol. 45, no. 8, pp. 830–837, Aug. 1998, doi: 10.1109/81.704822.



CHANGXI YUE was born in Xi'an, China, in 1982. He received the B.S. and M.S. degrees in electrical engineering from Xian Jiaotong University, Xi'an, in 2004 and 2006, respectively.

From 2008 to 2011, he was an Engineer with the State Grid Electric Power Research Institute. In 2011, he was a Guest Scientist with PTB. In 2012, he joined China Electric Power Research Institute (CEPRI). He currently leads the High-Voltage and High-Current Test Technique

Group, China Electric Power Research Institute, Wuhan, China. He is also a Senior Research Engineer experienced in high voltage and high current tests and measurements.



XIAODONG YIN (Senior Member, IEEE) received the B.S., M.S., and Ph.D. degrees in electrical engineering from Wuhan University.

He is currently with the Institute of Metrology, China Electric Power Research Institute. He mainly carries out research on frequency voltage proportional standard device and value traceability, metering secondary circuit inspection, and online monitoring of low-voltage current transformers. He has published more than 30 articles and granted

more than 50 invention patents in this field.

Dr. Yin was selected as a member of the "Young Talents Support Project" of the Chinese Electrical Engineering Society, in 2017. He was awarded the "Labor Award" of the Chinese Academy of Electrical Engineering, in 2020. He was awarded the title of "Model Worker" by CEC, in 2020, and the 23rd China Patent Gold Award, in 2022.



HAIBIN CHEN was born in Shanghai, China, in 1981. He received the master's degree in electronic science and technology from Zhejiang University, in 2006.

Since 2006, he has been with State Grid Shanghai Municipal Electric Power Company, where he is currently the Deputy Department Director. His primary responsibilities include technical research and management of energy metering equipment, such as instrument transformers.



KUI XIONG was born in Hunan, China, in 1988. He received the B.S. and M.S. degrees in detection technology and automatic equipment from North China Electric Power University, Beijing, China, in 2010 and 2013, respectively.

Since 2013, he has been with China Electric Power Research Institute (CEPRI), Wuhan, China, where he is currently a Senior Research Engineer working on current transformer calibration and current measurements.



HAOHAN ZHEN was born in Sichuan, China, in 1988. He received the master's degree in electrical engineering from Xi'an Jiaotong University, in 2013.

Since 2013, he has been with State Grid Shanghai Municipal Electric Power Company, where he specializes in technical management of energy metering equipment, including electricity meters and instrument transformers.